J Mater Sci (2015) 50:1006–1015
DOI 10.1007/s10853-014-8660-y

Effects of heating rates on microstructure and superplastic behavior of friction stir processed 7075 aluminum alloy

K. Wang · F. C. Liu · P. Xue · B. L. Xiao · Z. Y. Ma

Received: 9 July 2014 / Accepted: 8 October 2014 / Published online: 21 October 2014
© Springer Science+Business Media New York 2014

Abstract The effects of heating rate prior to tension on the microstructure and superplastic behavior of friction stir processed (FSP) 7075Al alloy, with an initial grain size of 6.2 μm, were investigated. Under both slow and fast heating rates, the FSP specimens exhibited excellent grain stability without abnormal growth at elevated temperatures up to 535 °C. At temperatures lower than 500 °C, both specimens exhibited similar microstructure and superplastic behavior. At 535 °C, specimens heated via slow heating rate exhibited worse superplasticity compared with those heated by fast heating rate, because of significantly coarsened second-phase particles after high temperature exposure for a long time, which blocked grain boundary sliding during superplastic deformation and resulted in a premature fracture of specimens. It was identified that fast heating rate can prevent the particle coarsening and thus the grain growth during heating process effectively, thereby favoring obtaining an excellent superplasticity at elevated temperatures.

Introduction

Superplasticity is defined as the ability of a polycrystalline material to exhibit, in a generally isotropic manner, very high tensile elongations prior to failure [1]. The superplasticity of metallic materials is of considerable interest because of its wide applications in fabricating complex-shaped workpieces [2]. The grain size of a metallic material is one of the most important factors that affect the superplasticity [3]. It has been well established that high superplastic ductility can be achieved in the metallic materials with grain sizes below 10 μm [4–6].

Furthermore, the thermal stability of the fine grains during preheating and superplastic deformation is another important factor for achieving high superplasticity. The thermal stability of the fine-grained alloys is influenced by the grain size and distribution, the grain boundary type, and the size and distribution of second-phase particles [7–11]. Previous studies showed that the addition of scandium or other rare earth elements to aluminum can generate a distribution of fine particles that substantially stabilize the fine-grained microstructure produced by severe plastic straining [11–14].

In addition to the microstructural characteristics and chemical composition of the alloys, the heating rate can also influence the stability of fine-grained alloys. Hassan et al. [10] found that when the heating rate was reduced, the fine-grained 7010Al alloy became progressively coarser with obviously discontinuous grain growth behavior.

For superplastic test, tensile specimens should be heated to a preset temperature at a certain heating rate and then held for a period to reach thermal equilibrium prior to tension. Generally, the tensile specimens can be heated to a preset temperature by different heating rates. For example, in a study by Ma et al. [15], the tensile specimens were fastened in the testing apparatus at room temperature, preheated to a preset temperature, and then held for 20 min to establish thermal equilibrium prior to tension. Similarly, Takayama et al. [16] heated the specimens to a given

K. Wang · F. C. Liu · P. Xue · B. L. Xiao · Z. Y. Ma (✉)
Shenyang National Laboratory for Materials Science, Institute of Metal Research, Chinese Academy of Sciences, 72 Wenhua Road, Shenyang 110016, China
e-mail: zyma@imr.ac.cn

K. Wang
College of Materials Science and Engineering, Chongqing University, 174 Shapinba Main Street, Chongqing 400030, China

temperature at a rate of 34.2 °C min^{-1} and then held at that temperature for 30 min. Komura et al. [17] also heated the specimens to the required temperature over a period of 30 min and held at that temperature for 10 min to establish thermal equilibrium.

On the other hand, fast heating was also used for superplastic test. For example, in the studies of Wang et al. [18] and Sotoudeh and Bate [19], the tensile specimens were directly put into the tensile tester which had been heated to the preset temperature in advance and then held at that temperature for 20 min. In Kim et al.'s study [20], the specimens were heated to the test temperature within only 5 min, and then kept at that temperature for 5 min before the tensile loading was initiated.

Our previous study [18] showed that friction stir processed (FSP) 7075Al alloy, which was heated to a preset temperatures in a short time, exhibited exceptionally high elongation of 3250 % at a high strain rate of 1×10^{-2} s^{-1} and 535 °C, which just a little exceeded the incipient melting temperature of this alloy (527 °C) [18]. In contrast, FSP 7075Al alloy, which was heated with a slow heating rate, did not show the same order of elongation at a high temperature of 530 °C [15]. This implies that the preheating rate for the tensile specimens might exert a significant effect on the superplastic behavior of fine-grained alloys. However, the detailed investigation in this subject is lacking in the literature.

In this study, the fine-grained 7075Al alloy produced by FSP was subjected to a detailed superplastic investigation at different preheating rates. The aim of the present work is to understand the effects of heating rates on the microstructure and superplastic behavior of fine-grained aluminum alloys.

Experimental

Commercial 7075Al-T651 rolled plates 8 mm thick, 70 mm wide, and 400 mm long with a nominal composition of 5.85Zn–2.56Mg–1.89Cu–0.22Cr (in wt%) were used. A single-pass FSP was carried out at a tool rotation rate of 1200 rpm and a traverse speed of 25 mm min^{-1}. The tool was manufactured from M42 steel with a concave shoulder 14 mm in diameter, and a threaded conical pin 5 mm in root diameter, 3.5 mm in tip diameter, and 4.0 mm in length.

Both the as-processed and the as-received aluminum plates were cut in the transverse direction, mounted, and mechanically polished for microstructural investigation. Keller's reagent was used to reveal the microstructures of these samples. Metallographic examination was completed using optical microscopy (OM), scanning electron microscopy (SEM, ZEISS SUPRA 35), and transmission electron microscopy (TEM, Tecnai G2). Thin foils for TEM were prepared by twin-jet polishing at −30 °C and 19 V using a solution of 30 % HNO_3 + 70 % methanol (vol%). The grain sizes were estimated by the linear intercept method.

To evaluate the superplastic behavior of FSP 7075Al, mini tensile specimens (2.5 mm gage length, 1.4 mm gage width, and 1.0 mm gage thickness) were electrodischarge machined perpendicular to the FSP direction, with the gage length being centered in the stirred zone. These specimens were subsequently ground and polished to a final thickness of ∼0.8 mm. Constant crosshead speed tensile tests were conducted using an Instron 5848 microtester.

To compare the effects of heating rates on the microstructure and superplasticity of the FSP 7075Al, two heating procedures were used: (i) Slow heating—putting the specimens into the furnace equipped on the tester at room temperature, preheating to the preset temperatures at a heating rate of 12.5 °C min^{-1}, and then holding for 20 min; (ii) fast heating—putting the specimens into the furnace that had been heated to the preset temperatures and then holding at that temperature for 20 min. The average heating rate of the specimens for the fast heating was determined to be ∼50 °C min^{-1}. Specimens heated by slow heating and fast heating processes are designated as "SHed specimen" and "FHed specimen" in this investigation, respectively.

Results

Microstructures

The microstructure of the rolled 7075Al was characterized by large elongated pancake-shaped grains (Fig. 1a). FSP generated significant frictional heating and extensive plastic deformation, thereby creating fine and equiaxed recrystallized grains in the FSP 7075Al (Fig. 1b). The average grain size in the FSP 7075Al, determined by the mean linear intercept technique, was 6.2 μm. TEM examinations indicated that the second-phase particles in the FSP 7075Al were uniformly distributed both at the grain boundaries and within the grains (Fig. 1c). Similar particles were identified by Mahoney et al. [21] as Cr-bearing dispersoids (dark color) and $MgZn_2$-type precipitates (bright color).

Microstructural evolution during heating

Figure 2a, c shows the EBSD micrographs of the FSP 7075Al heated to 535 °C at slow and fast heating rates, respectively. The grains of both specimens maintained equiaxed, and the average grain size was determined to be

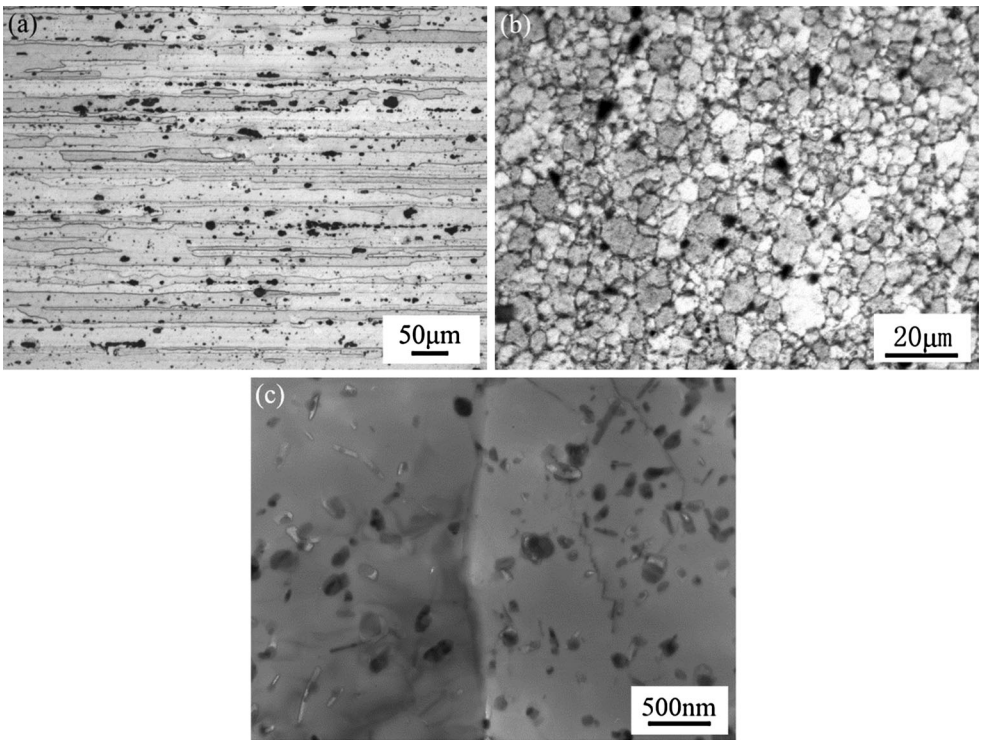

Fig. 1 **a** Optical micrograph showing large elongated pancake-shaped grains in rolled 7075Al, **b** optical micrograph showing fine and equiaxed grains in FSP 7075Al, and **c** TEM micrograph showing the distribution of second-phase particles in FSP 7075Al

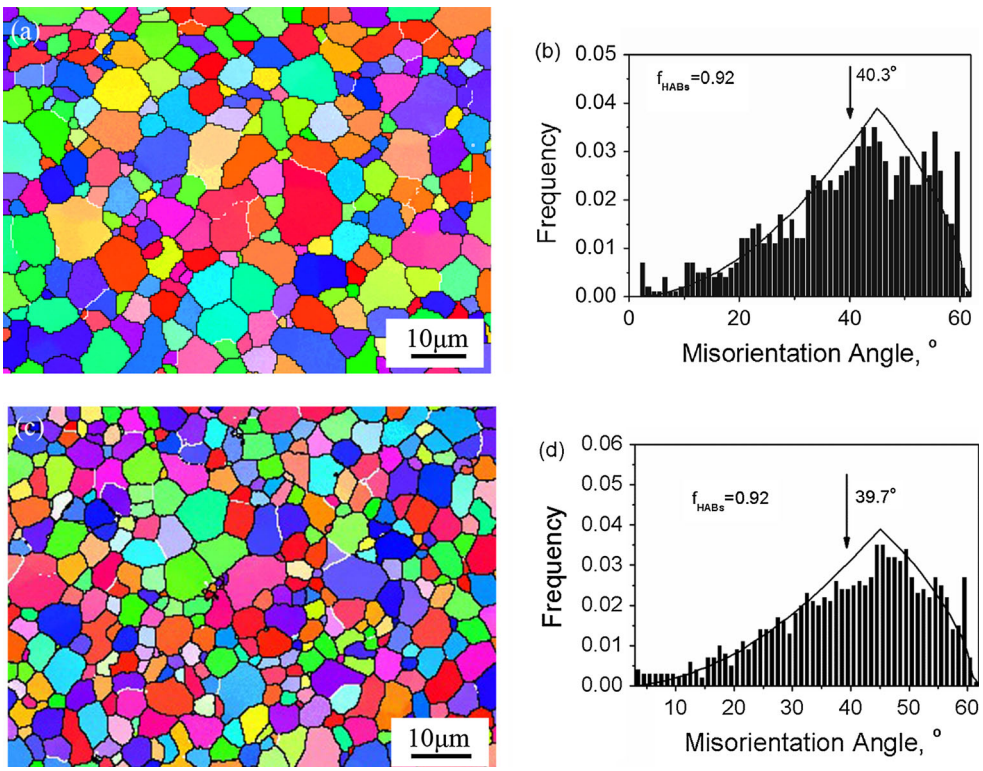

Fig. 2 EBSD maps and boundary misorientation angle distribution of FSP 7075Al annealed at 535 °C via **a**, **b** SH and **c**, **d** FH processes

10 and 6.9 μm for the SHed and FHed specimens, respectively, demonstrating that the FSP 7075Al exhibited excellent thermal stability. The misorientation angle histograms of the SHed and FHed specimens are shown in Fig. 2b, d. Both the SHed and FHed specimens exhibited the same fraction of high-angle grain boundaries (HAGBs)

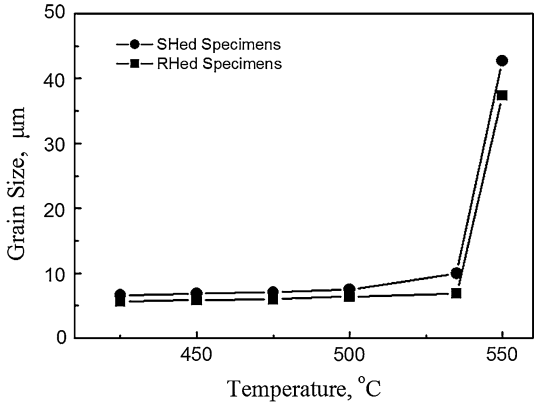

Fig. 3 Grain size versus annealing temperature for FSP 7075Al

of 92 %. Furthermore, the average misorientation angle of the SHed and FHed specimens was determined to be 40.3° and 39.7°, respectively, which are very close to the random grain assembly predicted by Mackenzie for randomly oriented cubes [22].

Figure 3 presents the variation of the average grain size of the FSP 7075Al subjected to slow heating and fast heating processes as a function of the annealing temperature. When the test temperature was lower than 500 °C, the grain growth rate was slow and there was no significant difference in the grain sizes between two specimens. When increasing the annealing temperature from 500 to 535 °C, the grain growth rate of the SHed specimen was faster than that of the FHed specimen. After further increasing the annealing temperature to 550 °C, both FHed and SHed specimens exhibited rapid grain growth.

Figure 4 shows the TEM micrographs of SHed and FHed specimens at 500 and 535 °C. Compared with the microstructure in the FSP sample (Fig. 1c), rod-liked metastable $MgZn_2$ precipitates were dissolved and the spherical Cr-bearing dispersoids were coarsened during preheating to elevated temperatures. Furthermore, the dispersoids in the SHed specimens were larger than that in the FHed specimens at the same test temperatures. An increase in the test temperature from 500 to 530 °C led to the growth of dispersoids from 171 to 195 nm for the SHed specimens and from 166 to 167 nm for the FHed specimens.

Superplastic properties

Figure 5 shows the variation of elongation-to-failure with initial strain rates for the FSP 7075Al at test temperatures of 450–535 °C. For the SHed specimens, the largest elongation of 2010 % was achieved at an initial strain rate of 3×10^{-3} s^{-1} and a deformation temperature of 500 °C. The largest elongation of 3250 % was obtained at a higher strain rate of 1×10^{-2} s^{-1} and a higher temperature of 535 °C in the FHed specimens.

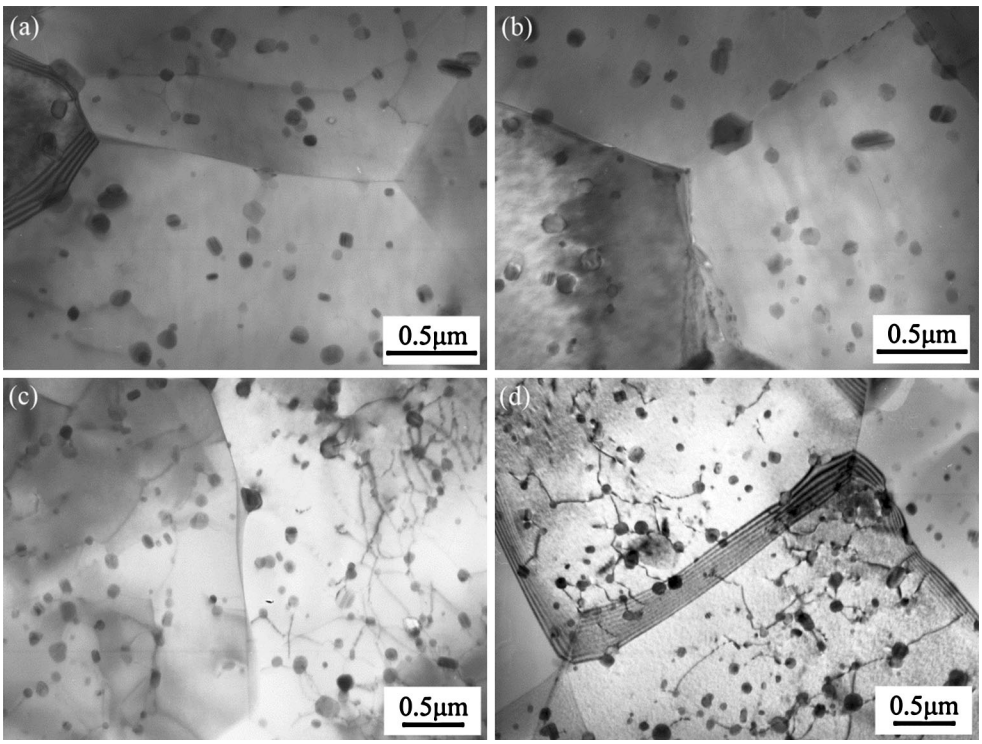

Fig. 4 TEM micrographs of FSP 7075Al preheated to **a** 500 °C via SH, **b** 535 °C via SH, **c** 500 °C via FH, and **d** 535 °C via FH processes

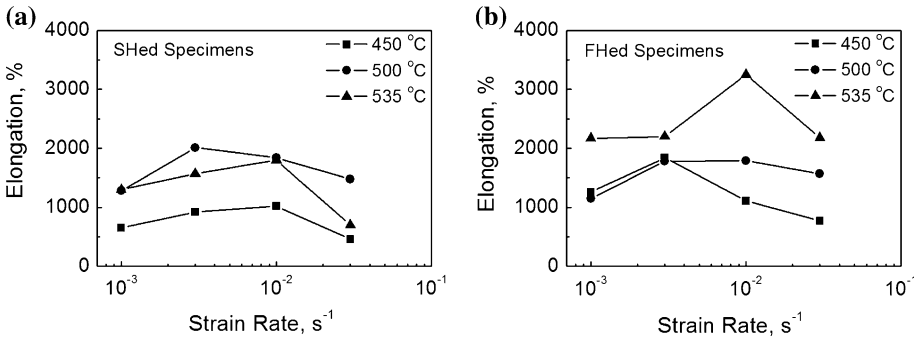

Fig. 5 Variation of elongation with initial strain rate for FSP 7075Al via **a** SH and **b** FH processes

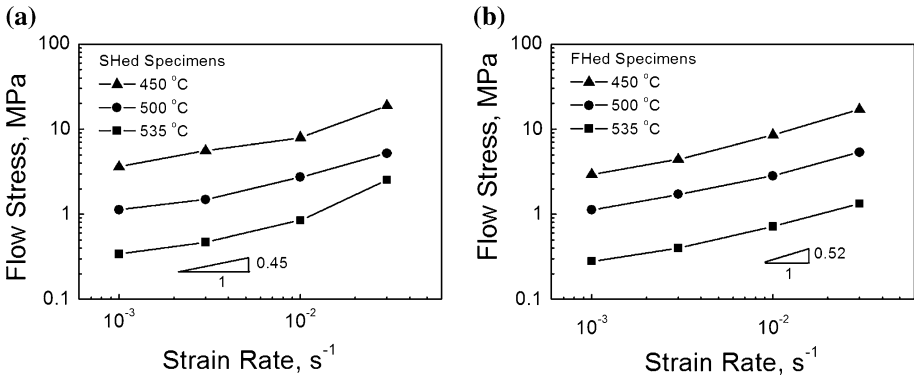

Fig. 6 Variation of flow stress with initial strain rate for FSP 7075Al via **a** SH and **b** FH processes

It is noted that the SHed specimens exhibited higher elongation than the FHed specimens at 500 °C and lower strain rates. Similar trends were also observed in the superplastic deformation of FSP Al–Mg–Sc alloys [23]. These results demonstrated that the optimum superplastic deformation rate of FSP aluminum alloys decreased with an increase in the grain size. However, the reduced superplastic deformation rate is beneficial to accommodating GBS and inhibiting the cavitation development during superplastic deformation. Therefore, it is possible that higher superplastic elongation was obtained at lower strain rates for FSP specimens with relatively large grain size.

The flow stress taken at a true strain of 0.1 is plotted as a function of strain rate on a double logarithmic scale in Fig. 6. For both the SHed and FHed specimens, high strain rate sensitivity (m) values of $\sim$0.5 were observed at the strain rates higher than 3×10^{-3} s^{-1} for all the investigated temperatures.

Figure 7 shows the failed tensile specimens tested at the optimum strain rates (3×10^{-3} s^{-1} for the SHed specimens and 1×10^{-2} s^{-1} for the FHed specimens) and various temperatures. The uniform deformation along the gage is a typical feature of superplastic deformation.

Microstructures near the fracture tips for the specimens deformed at an initial strain rate of 1×10^{-2} s^{-1} and temperatures of 500 and 535 °C are shown in Fig. 8, and the measurement results of the grain size are presented in Table 1. It is clear that the grain coarsening occurred during the superplastic deformation, and the grains were elongated along the tensile direction. The formation of large elongated cavities in the SHed specimens (Fig. 8a, b) and the FHed specimens (Fig. 8c) deformed at 500 °C was suggested as the plasticity controlled cavity growth, which resulted from the non-uniformity of grain boundary sliding (GBS) and incompatibility of plastic deformation between areas of equiaxed fine grains and areas of highly elongated grains [24].

In the SHed specimens deformed at 535 °C (Fig. 8b), the concentrated-type cavities as a result of cavity interlinkage were observed. It should be pointed out that the grains grew to 22.6 and 12.4 μm in the tension and transverse directions because of the concurrent grain growth during superplastic deformation. In contrast, the average grain size of the FHed specimens was grown to 28.7 and 12.8 μm in the tension and transverse directions, larger than the grain size of the SHed specimens (Table 1). Although the grains of the FHed specimens was significantly coarsened, only little cavitation was observed in the FHed specimens tested at 535 °C and 1×10^{-2} s^{-1}.

From the true stress–true strain curves presented in Fig. 9, it can be seen that both SHed and FHed specimens deformed at 535 °C exhibited a continuous stress hardening with the strain, which resulted in a pseudo-brittle type of failure at last. Comparatively, the flow stresses for both specimens deformed at 500 °C showed strain hardening up

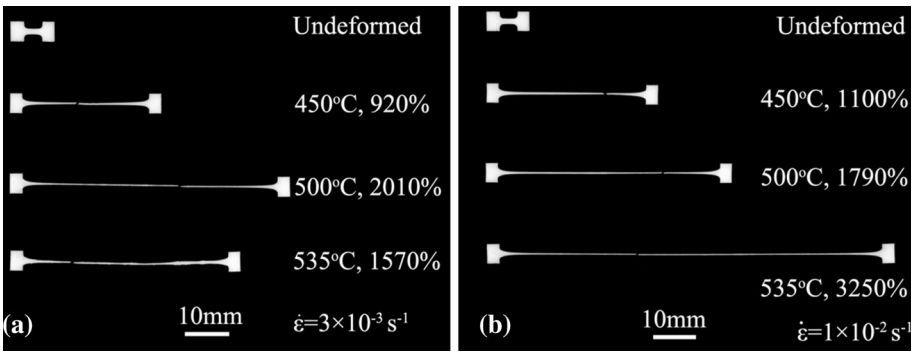

Fig. 7 Appearances of tensile specimens of FSP 7075Al after superplastic deformation: **a** SHed specimens at 3×10^{-3} s^{-1} and **b** FHed specimens at 1×10^{-2} s^{-1}

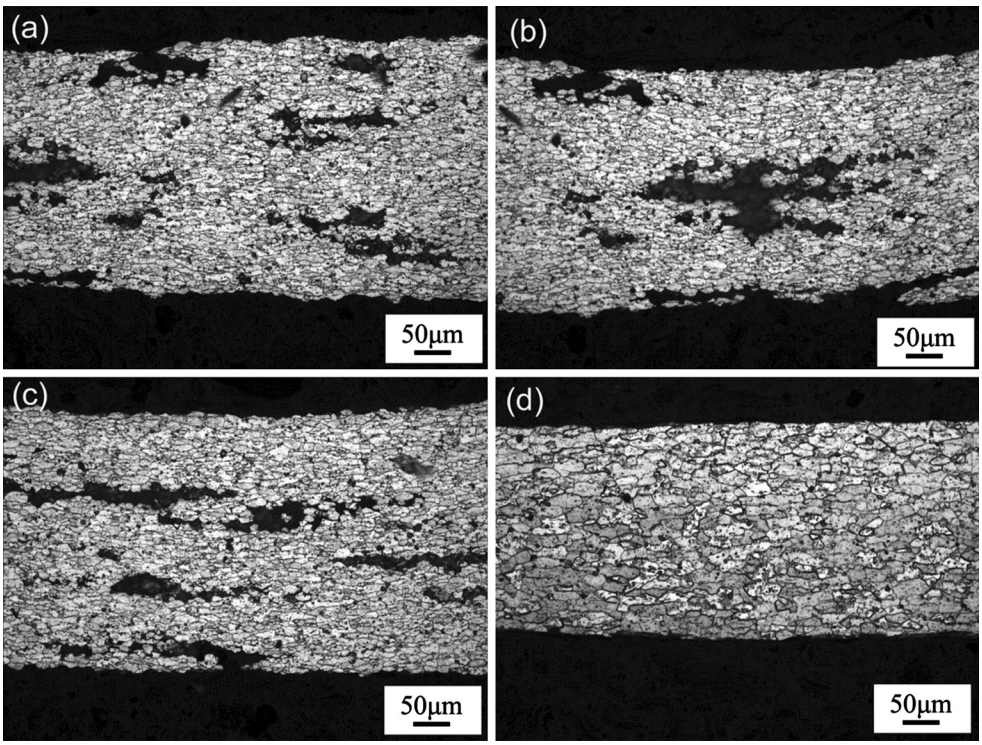

Fig. 8 Microstructures of superplastically deformed tensile specimens (1×10^{-2} s^{-1}) near the fracture tip (the tensile axis is *horizontal*): **a** SHed specimens at 500 °C, **b** SHed specimens at 535 °C, **c** FHed specimens at 500 °C, and **d** FHed specimens at 535 °C

Table 1 Grain size in the gage section in failed samples at $\dot{\varepsilon} = 1 \times 10^{-2}$ s^{-1}

Specimen	Temperature	
	500 °C	535 °C
L_d (μm)[a]		
SH	17.2/10.5	22.6/12.4
FH	26.9/13.1	28.7/12.8

[a] The numerator and denominator are the grain sizes measured in the tension and transverse directions, respectively

to a large strain prior to the maximum values, then the flow stresses continuously decreased until fracture. It is noted that the SHed specimens with relatively large grain size exhibited lower flow stresses at high strains. This should be attributed to the significant development of cavitation in the SHed specimens at large deformation stages (Fig. 8).

Discussion

Effects of heating rates on microstructures

The grains of the present FSP 7075Al coarsened both gradually and uniformly without any significant change in the misorientation distribution of contiguous grains and the fraction of HAGBs, as shown in Fig. 2. It was reported that when the fraction of HAGBs exceeded 0.6–0.7, the grain

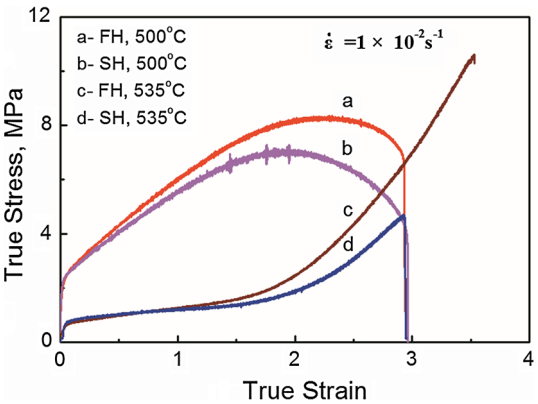

Fig. 9 True stress–true strain curves for FSP 7075Al preheated by SH and FH processes

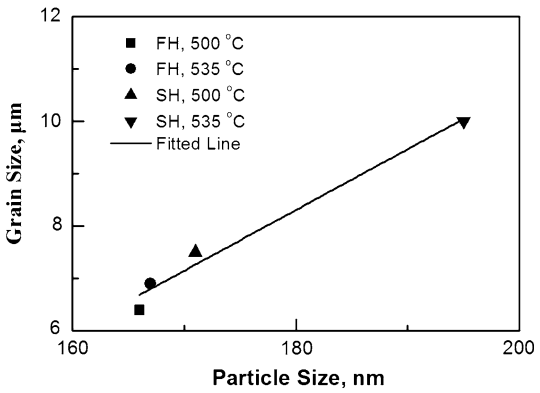

Fig. 10 Relationship between grain sizes and particle sizes for FSP 7075Al with different heating rates

microstructure had a great resistance to discontinuous grain coarsening [7, 8]. The present FSP microstructure was highly resistant to discontinuous grain coarsening at temperatures up to 535 °C (Fig. 2), which can be partly attributed to predominant HAGBs of about 90 %.

The continuous grain growth of fine-grained alloys is mainly controlled by curvature-driven grain-boundary migration (GBM) [25–27]. Furthermore, GBM was carried out by migration of atoms at the grain boundaries by diffusion. Similar to other particle-containing alloys [10], the final grain size in the present FSP 7075Al should also be influenced by the dispersion parameter (f/r, in which f is the particle volume fraction and r is the particle radius) via particle limiting grain size or Zener limit [8].

It has been known that particle coarsening usually happens with solute transport from dissolving smaller particles to the growing larger ones during heating [28–30], and lattice diffusion is the rate controlling step in the process. Slow heating rate led to a long exposure time at elevated temperatures; it took 40 and 10 min to heat specimens to the preset temperatures for the SHed and FHed specimens in this investigation, respectively. Therefore, it can be deduced that slow heating should result in an obvious coarsening of second-phase particles in the FSP 7075Al alloy, thereby reducing the dispersion parameter.

As seen in Fig. 4, when the preset heating temperature was 500 °C, the Cr-bearing dispersoids in the SHed and the FHed specimens were 171 and 166 nm, respectively. Once the preset heating temperature was increased to 535 °C, the dispersoids in the SHed specimens coarsened up to 195 nm rapidly, whereas the dispersoids in the FHed specimens exhibited a similar size to that at 500 °C. Therefore, the dispersion parameter of the Cr-bearing dispersoids in both specimens should be approximately the same at 500 °C, whereas the dispersion parameter in the SHed specimens at 535 °C decreased substantially for the coarsening of these Cr-bearing dispersoids. The high thermal stability of Cr-bearing dispersoids at elevated temperatures can be attributed to the high diffusion activation energy of Cr atom in the Al alloys [15, 31].

Correspondingly, the grains of the present FSP 7075Al exhibited a slow growth below 500 °C, and so did the FHed specimens at 535 °C. However, there was an obvious increase in the grain size for the SHed specimens at 535 °C (Fig. 3). This phenomenon implies that the grain size was controlled by the particle size, and a linear correlation between the grain size and particle size can be observed for the present FSP 7075Al (Fig. 10). Hence, the grain size was expected to be controlled by the growth rate of Cr-bearing dispersoids for the present FSP 7075Al, which is consistent with previous studies in Al–Sc [32] and Al–Ni alloys [33].

Effects of microstructure on superplasticity

To understand the effects of the microstructure on resultant superplasticity, it is necessary to compare the superplastic properties of the FSP 7075Al alloy heated via SH and FH processes. Figure 11 shows that the elongations of both specimens are similar below 500 °C, and that increasing heating rate resulted in a significantly enhanced elongation at 535 °C, a shift of optimum strain rate from 3×10^{-3} to 1×10^{-2} s^{-1}, and an increase of optimum deformation temperature from 500 to 535 °C.

GBS is the dominant superplastic deformation mechanism in fine-grained materials which is characterized by a stress exponent of ~ 2. The strain rate sensitivities of both SHed and FHed specimens at the optimal superplastic strain rate were about 0.5 (Fig. 6), corresponding to a stress exponent of ~ 2, which indicates that GBS is their dominant deformation mechanism. Such a low stress exponent value generally indicates higher resistance to neck-free

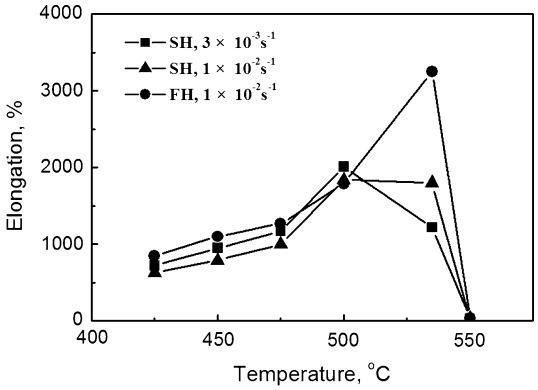

Fig. 11 Comparison of superplastic ductility between FHed and SHed 7075Al alloys as a function of deformation temperature

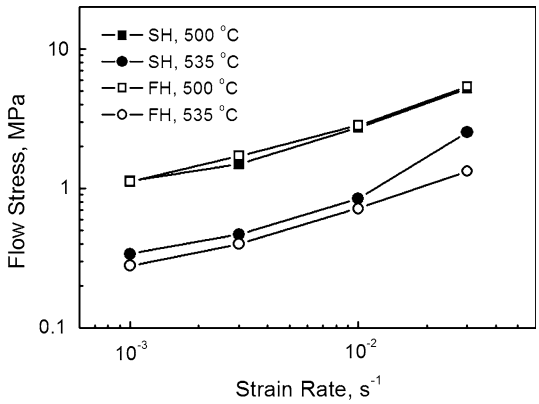

Fig. 12 Variation of flow stress with initial strain rate at 500 and 535 °C for FSP 7075Al

elongation, and Fig. 7 clearly shows uniform and neck-free deformation characteristics of the FSP 7075Al.

With the increase of grain size, a transition gradually appears from intergranular plastic deformation based GB accommodation to a mixture of intergranular and intragranular processes [34], so fine grain size is helpful for increasing GBS contribution and resulting in an enhanced superplasticity. The constitutive relationship for superplastic deformation of fine-grained aluminum alloys [15] also predicts that a grain size reduction to $0.32d$ (d, grain size) can increase the strain rate by a factor of 10. The initial grain size (6.9 μm) of the FHed specimen was 0.69 times of that (10 μm) of the SHed specimens in the present study. Therefore, the degree of grain size decrease should not result in an increase in the strain rates from 3×10^{-3} s^{-1} to 1×10^{-2} s^{-1}. This phenomenon indicates that other microstructural characteristics, such as grain boundary misorientation and second-phase particles, have also great effects on GBS [15, 35, 36]. Because the FSP 7075Al alloy in the present investigation makes little difference in the fraction of HAGBs and the grain boundary misorientation distributions via slow and fast heating processes (Fig. 2), it can be deduced that second-phase particles distributed at the grain boundaries affected the superplastic behavior of the FSP 7075Al.

Phenomenally, the grain boundaries slide in a viscous manner by a shear stress field [37, 38]. Raj and Ashby [39] considered that the particles distributed at the grain boundaries offer the resistance by blocking the otherwise free sliding which is further accommodated by diffusion around the particles. Physically, this blocking effect on GBS comes from the internal stress produced by the particle impeding GBS. Mori et al. [38] clarified the particle blocking effect on GBS through a mechanics analysis, and showed that relaxation strength is given by

$$\Delta = \Delta_0/(1 + \pi\beta r/\lambda^2), \tag{1}$$

where Δ_0 is the relaxation strength when the boundaries are free from the second-phase particles, β is the grain boundary radius, r is the radius of the blocking particles, and λ is the interparticle spacing.

Figure 12 compares the flow stresses of the SHed and the FHed specimens at 500 and 535 °C. At 500 °C, the flow stresses of both specimens were almost equal at various strain rates. However, at 535 °C, the flow stresses of the SHed specimens were 20 % higher than those of the FHed specimens. The changes of the flow stress corresponded to the microstructural variation of the specimens. As seen from Figs. 2, 3, and 4, there is similar grain size and second-phase particle size in both SHed and FHed specimens heated to 500 °C. When heating to 535 °C, the grain size and the particle size in the SHed specimens were 1.45 and 1.14 times larger than those in the FHed specimens, respectively, while the interparticle spacing of the SHed specimens was measured to be 1.37 times larger than that of the FHed specimens. Consequently, the flow stresses of the SHed specimens were higher than that of the FHed specimens at this temperature according to Eq. (1).

Moreover, when a small particle is introduced at the grain boundaries, the rate of accommodation would obviously depend on the size of the particle. If the particle size is below a critical size, the particle would not influence the nature of GBS. According to Stowell et al. [40], the critical strain rate, $\dot{\varepsilon}$, below which cavity nucleation at a grain boundary particle of radius, r_p, is likely to be inhibited by diffusive stress, is expressed by

$$\dot{\varepsilon} = \frac{2.9\sigma\Omega\delta D_b}{\alpha d r_p^2 kT}, \tag{2}$$

where σ is the stress required to nucleate a stable cavity, Ω is the atomic volume, δD_b is the product of grain boundary width and diffusivity, α is the fraction of the

total strain attributable to the GBS, d is the grain diameter, k is Boltzmann's constant, and T is the absolute temperature.

Equation (2) predicts that cavitation will be minimized when both grain and particle sizes are small. In the present study, the grain size in the failed SHed specimen (Fig. 8b; Table 1) was smaller than that in the failed FHed specimen tested at 535 °C (Fig. 8d; Table 1), and both specimens had similar strain-hardening behavior (Fig. 9). However, only in the failed SHed specimen could the concentrated-type cavities be observed. It was suggested that the size of the Cr-bearing dispersoids was beyond the critical size, which caused the occurrence of cavitation in the SHed specimen, and subsequently resulted in a premature failure and a comparatively low elongation. Similarly, Liu et al. [41] pointed out that the coarsening of second-phase particles resulted in a worse superplasticity.

The superplastic study of FSP 7075Al by Ma et al. [15] showed that the optimum elongation was obtained at the strain rate of 1×10^{-2} s^{-1} and the temperature of 470–490 °C, and an obvious decrease in elongation happened when the specimens were heated up to 530 °C. The change of superplastic behavior with temperature was similar to that of the SHed specimens in the present study, with slow heating used in both cases. In contrast, the specimens heated by fast heating exhibited significantly increased superplasticity up to 535 °C. Therefore, it can be concluded that fast heating rate obviously enhanced the superplastic properties of fine-grained alloys at elevated temperatures. In addition, fast hating rate can improve the process efficiency during superplastic forming.

Previous investigations showed that although the 7055Al alloy produced by equal channel angular extrusion (ECAE) had an average grain size of 1.4 μm, it only exhibited a maximum elongation of less than 1000 % at a temperature of 450 °C and an initial strain rate of 5.6×10^{-3} s^{-1} [42, 43]. In contrast, maximum elongations higher than 1000 % have been extensively observed in the FSP 7075Al alloys with average grain sizes of 3–10 μm [15, 18, 44, 45]. The achievement of higher elongation in the FSP 7075Al alloys can be attributed to two factors. First, the FSP 7075 Al exhibited better thermal stability at the elevated temperatures due to its relatively large grain size. Therefore, the superplastic deformation can be conducted at higher temperatures which accelerated the atom diffusion process to well accommodate GBS. Second, the fraction of HAGBs in the FSP 7075Al alloys was usually higher than 90 % [18, 44], which is much higher than that obtained in the ECAE 7075Al with a typical fraction of 67 % [43]. The extremely high fraction of HAGBs in the FSP 7075Al alloys enhanced the GBS during high temperature deformation.

Conclusions

(1) Fine-grained 7075Al with a grain size of 6.2 μm prepared by FSP exhibited excellent thermal stability under different heating rates due to the strong pinning effect of second-phase particles, and the microstructures went through a continuous grain growth at elevated temperatures up to 535 °C.

(2) Both specimens heated by slow and fast heating rates had similar grain size and particle size below 500 °C. When the heating temperature reached 535 °C, the grains of the SHed specimen grew to 10 μm due to the coarsening of pinning second-phase particles. Increasing the heating rate could inhibit the coarsening of second-phase particles and the growth of grains by decreasing solution diffusion time.

(3) The FSP 7075Al exhibited excellent superplasticity under the investigated temperature range of 450–535 °C, and the optimum strain rate increased with increasing the heating rate. The optimum superplasticity of 3250 % was obtained in the FHed specimens at 1×10^{-2} s^{-1} and 535 °C, while the optimum superplasticity of >2000 % in the SHed specimens was observed at 3×10^{-3} s^{-1} and 500 °C, attributable to the larger sizes of the second-phase particles and grains.

Acknowledgements This work was supported by the National Natural Science Foundation of China under Grant Nos. 50871111 and 51331008.

References

1. Langdon TG, Wadsworth J (1991) Fatigue properties of SPF/DB joints in titanium alloys. In: Hori S, Tokizane M, Furushiro N (eds) Superplasticity in advanced materials. The Japan Society for Research on Superplasticity, Osaka, p 847
2. Barnes AJ (1994) Superplastic forming of aluminum alloys. Mater Sci Forum 170–172:701–714
3. Mishra RS, Bieler TR, Mukherjee AK (1995) Superplasticity in powder metallurgy aluminum alloys and composites. Acta Metall Mater 43:877–891
4. Langdon TG (1982) The mechanical properties of superplastic materials. Metall Mater Trans A 13:689–701
5. Liu FC, Xue P, Ma ZY (2012) Microstructural evolution in recrystallized and unrecrystallized Al–Mg–Sc alloys during superplastic deformation. Mater Sci Eng A 547:55–63
6. Liu FC, Ma ZY, Zhang FC (2012) High strain rate superplasticity in a micro-grained Al–Mg–Sc alloy with predominant high angle grain boundaries. J Mater Sci Technol 28:1025–1030
7. Humphreys FJ (1997) A unified theory of recovery, recrystallization and grain growth, based on the stability and growth of cellular microstructures—I. The basic model. Acta Mater 45:4231–4240
8. Humphreys FJ (1997) A unified theory of recovery, recrystallization and grain growth, based on the stability and growth of

cellular microstructures—II. The effect of second-phase particles. Acta Mater 45:5031–5039
9. Charit I, Mishra RS (2005) Low temperature superplasticity in a friction-stir-processed ultrafine grained Al–Zn–Mg–Sc alloy. Acta Mater 53:4211–4223
10. Hassan KAA, Norman AF, Price DA, Prangnell PB (2003) Stability of nugget zone grain structures in high strength Al-alloy friction stir welds during solution treatment. Acta Mater 51: 1923–1936
11. Naga Raju P, Srinivasa Rao K, Reddy GM, Kamaraj M, Prasad Rao K (2007) Microstructure and high temperature stability of age hardenable AA2219 aluminium alloy modified by Sc, Mg and Zr additions. Mater Sci Eng A 464:192–201
12. Forbord B, Hallem H, Røyset J, Marthinsen K (2008) Thermal stability of $Al_3(Sc_x, Zr_{1-x})$-dispersoids in extruded aluminium alloys. Mater Sci Eng A 475:241–248
13. Kumar N, Mishra RS (2012) Thermal stability of friction stir processed ultrafine grained AlMgSc alloy. Mater Charact 74:1–10
14. Lee S, Utsunomiya A, Akamatsu H, Neishi K, Furukawa M, Horita Z, Langdon TG (2002) Influence of scandium and zirconium on grain stability and superplastic ductilities in ultrafine-grained Al–Mg alloys. Acta Mater 50:553–564
15. Ma ZY, Mishra RS, Mahoney MW (2002) Superplastic deformation behaviour of friction stir processed 7075Al alloy. Acta Mater 50:4419–4430
16. Takayama Y, Tozawa T, Kato H (1999) Superplasticity and thickness of liquid phase in the vicinity of solidus temperature in a 7475 aluminum alloy. Acta Mater 47:1263–1270
17. Komura S, Furukawa M, Horita Z, Nemoto M, Langdon TG (2001) Optimizing the procedure of equal-channel angular pressing for maximum superplasticity. Mater Sci Eng A 297: 111–118
18. Wang K, Liu FC, Ma ZY, Zhang FC (2011) Realization of exceptionally high elongation at high strain rate in a friction stir processed Al–Zn–Mg–Cu alloy with the presence of liquid phase. Scripta Mater 64:572–575
19. Sotoudeh K, Bate PS (2010) Diffusion creep and superplasticity in aluminium alloys. Acta Mater 58:1909–1920
20. Kim WJ, Lee BH, Lee JB, Lee MJ, Park YB (2010) Synthesis of high-strain-rate superplastic magnesium alloy sheets using a high-ratio differential speed rolling technique. Scripta Mater 63:772–775
21. Mahoney MW, Rhodes CG, Flintoff JG, Bingel WH, Spurling RA (1998) Properties of friction-stir-welded 7075 T651 aluminum. Metall Mater Trans A 29:1955–1964
22. Mackenzie JK (1958) Second paper on statistics associated with the random disorientataion of cubes. Biometrica 45:229–240
23. Liu FC, Ma ZY (2011) Superplasticity governed by effective grain size and its distribution in fine-grained alumium alloys. Mater Sci Eng A 530:548–558
24. Kaibyshev R, Musin F, Lesuer DR, Nieh TG (2003) Superplastic behavior of an Al–Mg alloy at elevated temperatures. Mater Sci Eng A 342:169–177
25. Harris KE, Singh VV, King AH (1998) Grain rotation in thin films of gold. Acta Mater 46:2623–2633
26. Tengen TB, Wejrzanowski T, Iwankiewicz R, Kurzydłowski KJ (2007) Statistical model of grain growth in polycrystalline nanomaterials. Solid State Phenom 129:157–163
27. Trautt ZT, Mishin Y (2012) Grain boundary migration and grain rotation studied by molecular dynamics. Acta Mater 60:2 407–2424
28. Greenwood GW (1956) The growth of dispersed precipitates in solutions. Acta Metall 4:243–248
29. Lifshitz IM, Slyozov VV (1961) The kinetics of precipitation from supersaturated solid solutions. J Phys Chem Solids 19:35–50
30. Wagner CZ (1961) Theorie der Alterung von Niederschlagen durch umlosen. Elektrochem 65:581–583
31. Simonovic D, Sluiter MH (2009) Impurity diffusion activation energies in Al from first principles. Phys Rev B 79:054304-1–054304-12
32. Ferry M, Hamilton NE, Humphreys FJ (2005) Continuous and discontinuous grain coarsening in a fine-grained particle-containing Al–Sc alloy. Acta Mater 53:1097–1109
33. Humphreys FJ, Chan HM (1996) Discontinuous and continuous annealing phenomena in aluminium–nickel alloy. Mater Sci Technol 12:143–148
34. Van Swygenhoven H (2002) Grain boundaries and dislocations. Science 296:66–67
35. Ma ZY, Mishra RS, Mahoney MW, Grimes R (2003) High strain rate superplasticity in friction stir processed Al–Mg–Zr alloy. Mater Sci Eng A 351:148–153
36. Horton CAP (1972) Some observations of grain boundary sliding in the presence of second phase particles. Acta Metall 20: 477–484
37. Monzen R, Futakuchi M, Miura H (1993) Effect of an element addition on relaxation of elastic distortion based on particle-blocked grain boundary sliding. Scripta Metall Mater 29:563–566
38. Mori T, Koda M, Monzen R, Mura T (1983) Particle blocking in grain boundary sliding and associated internal friction. Acta Metall 31:275–283
39. Raj R, Ashby MF (1971) On grain boundary sliding and diffusional creep. Metall Mater Trans B 2:1113–1127
40. Stowell MJ (1982) In: Paton NE, Hamilton CH (eds) Superplastic forming of structural alloys. TMS-AIME, Warrendale, pp 321–336
41. Liu FC, Xiao BL, Wang K, Ma ZY (2010) Investigation of superplasticity in friction stir processed 2219Al alloy. Mater Sci Eng A 527:4191–4196
42. Kaibyshev R, Sakai T, Nikulin I, Musin F, Goloborodko A (2003) Superplasticity in a 7055 aluminum alloy subjected to intense plastic deformation. Mater Sci Technol 19:1491–1497
43. Nikulin I, Kaibyshev R, Sakai T (2005) Superplasticity in a 7055 aluminum alloy processed by ECAE and subsequent isothermal rolling. Materi Sci Eng A 407:62–70
44. Mishra RS, Mahoney MW, McFadden SX, Mara NA, Mukherjee AK (1999) High strain rate superplasticity in a friction stir processed 7075 Al alloy. Scripta Mater 42:163–168
45. Johannes LB, Mishra RS (2007) Multiple passes of friction stir processing for the creation of superplastic 7075 aluminum. Mater Sci Eng A 464:255–260